研究成果の刊行に関する一覧表レイアウト

書籍

なし

雑誌

発表者氏名	論文タイトル名	発表誌名	巻号	ページ	出版年
林 拓也, 大西 隆, 石田 康, 宇川 義一, 飯田 秀博	経頭蓋磁気刺激効果のPETによる研究	*神経内科*	62 (1)	5-10.	2005
Takagi Y, Takahashi J, Saiki H, Morizane A, Hayashi T, Kishi Y, Fukuda H, Okamoto Y, Koyanagi M, Ideguchi M, Hayashi H, Imazato T, Kawasaki H, Suemori H, Omachi S, Iida H, Itoh N, Nakatsuji N, Sasai Y, Hashimoto N	Dopaminergic neurons generated from monkey embryonic stem cells function in a Parkinson primate model.	*The Journal of Clinical Investigation*	115 (1)	102-109	2005
Kudomi N, Hayashi T, Teramoto N, Watabe H, Kawachi N, Ohta Y, Kim KM,Iida H	Rapid quantitative measurement of CMRO(2) and CBF by dual administration of (15)O-labeled oxygen and water during a single PET scan-a validation study and error analysis in anesthetized monkeys.	*J Cereb Blood Flow Metab*	25	1209-1224	2005
Ogawa, M, Watabe, H, Teramoto, N, Miyake, Y, Hayashi, T, Iida, H, Murata, T, Magata, Y	Understanding of cerebral energy metabolism by dynamic living brain slice imaging system with [18F]FDG.	*Neurosci Res*	52 (4)	357-61	2005

Suzuki A, Tashiro M, Kimura Y, Mochizuki H, Ishii K, Watabe H, Yanai K, Ishiwata K, Ishii K	Use of reference tissue models for quantification of histamine H1 receptors in human brain by using positron emission tomography and [11C]doxepin.	*Ann Nucl Med*	19 (6)	425-433	2005
Hirao K, Ohnishi T, Hirata Y, Yamashita F, Mori T, Moriguchi Y, Matsuda H, Nemoto K, Imabayashi E, Yamada M, Iwamoto T, Arima K, Asada T	The prediction of rapid conversion to Alzheimer's disease in mild cognitive impairment using regional cerebral blood flow SPECT.	*Neuroimage*	28(4)	1014-21	2005
Sakai Y, Kumano H, Nishikawa M, Sakano Y, Kaiya H, Imabayashi E, Ohnishi T, Matsuda H, Yasuda A, Sato A, Diksic M, Kuboki T.	Cerebral glucose metabolism associated with a fear network in panic disorder.	*Neuroreport*	16(9)	927-31	2005
Hirata Y, Matsuda H, Nemoto K, Ohnishi T, Hirao K, Yamashita F, Asada T, Iwabuchi S, Samejima H.	Voxel-based morphometry to discriminate early Alzheimer's disease from controls	*Neurosci Lett*	382(3)	269-74	2005
Moriguchi Y, Ohnishi T, Kawachi T, Mori T, Hirakata M, Yamada M, Matsuda H, Komaki G	Specific brain activation in Japanese and Caucasian people to fearful faces.	*Neuroreport*	16(2)	133-6	2005

Hiroki M, Uema T, Kajimura N, Ogawa K, Nishikawa M, Kato M, Watanabe T, Nakajima T, Takano H, Imabayashi E, Ohnishi T, Takayama Y, Matsuda H, Uchiyama M, Okawa M, Takahashi K, Fukuyama H	Cerebral white matter blood flow is constant during human non-rapid eye movement sleep: a positron emission tomographic study.	*J Appl Physiol*	98(5)	1846-54	2005
Ohnishi T, Hashimoto R, Mori T, Nemoto K, Moriguchi Y, Iida H, Noguchi H, Nakabayashi T, Hori H, Ohmori M, Tsukue R, Anami K, Hirabayashi N, Harada S, Arima K, Saitoh O, Kunugi H	The association between the Val158Met polymorphism of the catechol-O-methyl transferase gene and morphological abnormalities of the brain in chronic schizophrenia.	*Brain*	129 (Pt 2)	399-410	2006
Temma T, Magata Y, Kuge Y, Shimonaka S, Sano K, Katada Y, Kawashima H, Mukai T, Watabe H, Iida H, Saji H	Estimation of oxygen metabolism in a rat model of permanent ischemia using positron emission tomography with injectable(15)O-O(2).	*J Cereb Blood Flow Metab*	26 (12)	1577-1583	2006
Shimamura M, Sato N, Waguri S, Uchiyama Y, Hayashi T, Iida H, Nakamura T, Ogihara T, Kaneda Y, Morishita R	Gene transfer of hepatocyte growth factor gene improves learning and memory in the chronic stage of cerebral infarction	*Hypertension*	47 (4)	742-51	2006
林 拓也	拡散テンソルに基づくMRI画像の進歩 3. 大脳皮質・深部灰白質間の線維連絡.	*神経内科*	65 (2)	161-168	2006

Shidahara M, Inoue K, Maruyama M, Watabe H, Taki Y, Goto R, Okada K, Kinomura S, Osawa S, Onishi Y, Ito H, Arai H, Fukuda H	Predicting human performance by channelized Hotelling observer in discriminating between Alzheimer's dementia and controls using statistically processed brain perfusion SPECT	*Ann Nucl Med*	20 (9)	605-13	2006
越野 一博, 渡部 浩司, 飯田 秀博	ＰＥＴによる脳・心臓循環代謝イメージング.	*クリニカルプラクティス*	25 (12)	1135-1138	2006
Hashimoto R, Numakawa T, Ohnishi T, Kumamaru E, et al	Impact of the DISC1 Ser704Cys polymorphism on risk for major depression, brain morphology and ERK signaling.	*Hum Mol Genet*	15(20)	3024-33	2006
Ugawa Y, Okabe S, Hayashi T, Ohnishi T, Nonaka Y	Repetitive transcranial magnetic stimulation (rTMS) in monkeys.	*Suppl Clin Neurophysiol*	59	173-81	2006
Sakai Y, Kumano H, Nishikawa M, Sakano Y, Kaiya H, Imabayashi E, Ohnishi T	Changes in cerebral glucose utilization in patients with panic disorder treated with cognitive-behavioral therapy.	*Neuroimage*	33(1)	218-26	2006
Moriguchi Y, Ohnishi T, Lane RD, et al	Impaired self-awareness and theory of mind: an fMRI study of mentalizing in alexithymia.	*Neuroimage*	32(3)	1472-82	2006
Ohnishi T, Matsuda H, Hirakata M, Ugawa Y	Navigation ability dependent neural activation in the human brain: an fMRI study	*Neurosci Res*	55(4)	361-9	2006

Hashimoto R, Hattori S, Chiba S, Yagasaki Y, Okada T, Kumamaru E, Mori T, Nemoto K, Tanii H, Hori H, Noguchi H, Numakawa T, Ohnishi T, Kunugi H	Susceptibility genes for schizophrenia.	*Psychiatry Clin Neurosci*	60 Suppl 1	S4-S10.7	2006
Hirao K, Ohnishi T, Matsuda H, Nemoto K, Hirata Y, Yamashita F, Asada T, Iwamoto T	Functional interactions between entorhinal cortex and posterior cingulated cortex at the very early stage of Alzheimer's disease using brain perfusion single-photon emission computed tomography.	*Nucl Med Commun*	27(2)	151-6	2006
Nemoto K, Ohnishi T, Mori T, Moriguchi Y, Hashimoto R, Asada T, Kunugi H	The Val66Met polymorphism of the brain-derived neurotrophic factor gene affects age-related brain morphology.	*Neurosci Lett*	397(1-2)	25-9	2006
Masataka N, Ohnishi T, Imabayashi E, Hirakata M, Matsuda H.	Neural correlates for numerical processing in the manual mode.	*J Deaf Stud Deaf Educ*	11(2)	144-52	2006
Hiroki M, Kajimura N, Uema T, Ogawa K, Nishikawa M, Kato M, Watanabe T, Nakajima T, Takano H, Imabayashi E, Ohnishi T, Takayama Y, Matsuda H, Uchiyama M, Okawa M, Takahashi K, Fukuyama H	Effect of benzodiazepine hypnotic triazolam on relationship of blood pressure and Paco2 to cerebral blood flow during human non-rapid eye movement sleep.	*J Neurophysiol*	95(4)	2293-303	2006

飯田 秀博, 渡部 浩司, 赤松 哲哉, 中澤 真弓, 松原 圭亮, 竹内 朝子, 岩田 倫明, 林 拓也, 横田 千晶, 福島 和人, 福本 真司	SPECTを使った脳機能画像の定量化と標準化	*脳神経外科ジャーナル*	16 (10)	742-752	2007
林　拓也	ヒトの大脳皮質基底核連絡線維.	*Clinical Neuroscience*	25(1)	28-33	2007
林　拓也	大脳基底核と皮質の神経線維結合－拡散強調画像による検討	*臨床神経学*	47(11)	838-840	2007
生駒 洋子	PETを用いた脳内神経受容体の定量評価	*Medical Imaging Technology*	26 (1)	26-31	2007
圓見 純一郎	MR Perfusion 解析の進歩	*Medical Imaging Technology*	26 (1)	32-38	2007
Kudomi N, Watabe H, Hayashi T, Iida H	Separation of input function for rapid measurement of quantitative CMRO2 and CBF in a single PET scan with a dual tracer administration method.	*Phys Med Biol*	52(7)	1893-1908	2007
Shimamura M, Sato N, Sata M, Kurinami H, Takeuchi D, Wakayama K, Hayashi T, Iida H, Morishita R	Delayed Postischemic Treatment With Fluvastatin Improved Cognitive Impairment After Stroke in Rats.	*Stroke*	38(12)	3251-3258	2007
佐藤 博司, 稲垣 正司, 林 拓也, 飯田 秀博	目でみるページ・検査-diffusion MRI-.	*CARDIAC PRACTICE*		201-204	2007

Saito N, Kudo K, Sasaki T, Uesugi M, Koshino K, Miyamoto M, Suzuki S	Realization of reliable cerebral-blood-flow maps from low-dose CT perfusion images by statistical noise reduction using nonlinear diffusion filtering	*Radiological Physics and Technology*	1 (1)	62-74	2007
Mori T, Ohnishi T, Hashimoto R, Nemoto K, Moriguchi Y, Noguchi H, Nakabayashi T, Hori H, Harada S, Saitoh O, Matsuda H, Kunugi H	Progressive changes of white matter integrity in schizophrenia revealed by diffusion tensor imaging	*Psychiatry Research: Neuroimaging*	154(2)	133-45	2007
Moriguchi Y, Ohnishi T, Mori T, Matsuda H, Komaki G	Changes of brain activity in the neural substrates for theory of mind during childhood and adolescence	*Psychiatry Clin Neurosci*	61(4)	355-63	2007
Hashimoto R, Hashimoto H, Shintani N, Chiba S, Hattori S, Okada T, Nakajima M, Tanaka K, Kawagishi N, Nemoto K, Mori T, Ohnishi T, Noguchi H, Hori H, Suzuki T, Iwata N, Ozaki N, Nakabayashi T, Saitoh O, Kosuga A, Tatsumi M, Kamijima K, Weinberger DR, Kunugi H, *Baba A*	Pituitary adenylate cyclase-activating polypeptide is associated with schizophrenia.	*Mol Psychiatry*	12(11)	1026-32	2007
Iida H, Eberl S, Kim KM, Tamura Y, Ono Y, Nakazawa M, S Antti, Zeniya T, Hayashi T, Watabe H	Absolute quantitation of myocardial blood flow with 201Tl and dynamic SPECT in canine: optimisation and validation of kinetic modelling.	*Eur J Nucl Med Mol Imaging*			2007

Moriguchi Y, Decety J, Ohnishi T, Maeda M, Mori T, Nemoto K, Matsuda H, Komaki G	Empathy and judging other's pain: an fMRI study of alexithymia.	*Cereb Cortex*	17(9)	2223-34	2007
Yokoyama I, Inoue Y, Kinoshita T, Itoh H, Kanno I,Iida H	Heart and Brain Circulation and CO2 in Healthy Men	*Acta Physiol (Oxf)*	Feb.12	1748-1716	2008
Sato H, Enmi J, Teramoto N, Hayashi T, Yamamoto A, Tsuji T, Naito H, Iida H	Comparison of Gd-DTPA-induced signal enhancements in rat brain C6 glioma among different pulse sequences in 3-Tesla magnetic resonance imaging.	*Acta Radiol*	49 (2)	172-9	2008
Hashimoto R, Mori T, Nemoto K, Moriguchi Y, Noguchi H, Nakabayashi T, Hori H, Harada S, Kunugi H, Saitoh O, Ohnishi T.	Abnormal microstructures of the basal ganglia in schizophrenia revealed by diffusion tensor imaging.	*The World Journal of Biological Psychiatry*	In press		

 Related Commentary, page 23

Dopaminergic neurons generated from monkey embryonic stem cells function in a Parkinson primate model

Yasushi Takagi,[1,2] Jun Takahashi,[1] Hidemoto Saiki,[3] Asuka Morizane,[1] Takuya Hayashi,[4] Yo Kishi,[1] Hitoshi Fukuda,[1] Yo Okamoto,[1] Masaomi Koyanagi,[1] Makoto Ideguchi,[1] Hideki Hayashi,[1] Takayuki Imazato,[1] Hiroshi Kawasaki,[5] Hirofumi Suemori,[6] Shigeki Omachi,[7] Hidehiko Iida,[4] Nobuyuki Itoh,[7] Norio Nakatsuji,[6] Yoshiki Sasai,[2,5] and Nobuo Hashimoto[1]

[1]Department of Neurosurgery, Kyoto University Graduate School of Medicine, Kyoto, Japan. [2]Organogenesis and Neurogenesis Group, Center for Developmental Biology, RIKEN, Kobe, Japan. [3]Department of Neurology, Kyoto University Graduate School of Medicine, Kyoto, Japan. [4]Department of Experimental Radiology, National Cardiovascular Center, Osaka, Japan. [5]Department of Medical Embryology and Neurobiology and [6]Department of Development and Differentiation, Institute for Frontier Medical Sciences, Kyoto University, Kyoto, Japan. [7]Department of Genetic Biochemistry, Kyoto University Graduate School of Pharmaceutical Sciences, Kyoto, Japan.

Parkinson disease (PD) is a neurodegenerative disorder characterized by loss of midbrain dopaminergic (DA) neurons. ES cells are currently the most promising donor cell source for cell-replacement therapy in PD. We previously described a strong neuralizing activity present on the surface of stromal cells, named stromal cell–derived inducing activity (SDIA). In this study, we generated neurospheres composed of neural progenitors from monkey ES cells, which are capable of producing large numbers of DA neurons. We demonstrated that FGF20, preferentially expressed in the substantia nigra, acts synergistically with FGF2 to increase the number of DA neurons in ES cell–derived neurospheres. We also analyzed the effect of transplantation of DA neurons generated from monkey ES cells into 1-methyl-4-phenyl-1,2,3,6-tetrahydropyridine–treated (MPTP-treated) monkeys, a primate model for PD. Behavioral studies and functional imaging revealed that the transplanted cells functioned as DA neurons and attenuated MPTP-induced neurological symptoms.

Introduction

Parkinson disease (PD) is a neurodegenerative disorder characterized by the loss of midbrain dopaminergic (DA) neurons, with subsequent reductions in striatal dopamine levels. While initial pharmacological treatment with L-dihydroxyphenylalanin (L-DOPA) can attenuate symptoms, the efficacy of this treatment gradually decreases over time. The development of motor complications then requires additional treatments, including deep brain stimulation and fetal DA neuron transplantation (1–3). Both studies of animal models and clinical investigations have shown that transplantation of fetal DA neurons can produce symptomatic relief (4–8). The technical and ethical difficulties in obtaining sufficient and appropriate donor fetal brain tissue, however, have limited the application of this therapy.

ES cells are self-renewing, pluripotent cells derived from the inner cell mass of the preimplantation blastocyst. These cells have many of the characteristics required of a cell source for cell-replacement therapy, including proliferation and differentiation capacities (9). We previously discovered that a strong neuralizing activity, which we called stromal cell–derived inducing activity (SDIA), is present on the surface of stromal cells. In the absence of exogenous bone morphogenic protein–4, mouse ES cells differentiate efficiently into neural precursors and neurons when cultured for 1 week on SDIA-expressing mouse stromal cells (PA6 cells) (10). Recently, SDIA induction has also been applied to primate ES cells, which generated large numbers of neural precursors and postmitotic neurons when cultured on PA6 cells for two weeks (11). The SDIA method is both technically simple and efficient, producing significant numbers of midbrain DA neurons (10, 11).

Self-renewing, multipotent neural progenitors can be cultured as neurospheres (12). In this study, we generated neural progenitors from monkey ES cells, then expanded them as neurospheres, which contained progenitors of DA neurons. In addition, we analyzed the effect of FGF20, a novel member of the FGF family of growth factors that is expressed exclusively in the substantia nigra of the brain and is reported to have a protective effect on DA neurons (13). We observed increased DA neuron induction following treatment with FGF20. Furthermore, we transplanted neurons generated by this method into 1-methyl-4-phenyl-1,2,3,6-tetrahydropyridine–treated (MPTP-treated) cynomolgus monkeys, a primate model for PD. We found that transplanted cells were able to function as DA neurons and could diminish Parkinsonian symptoms. This is the first report, to our knowledge, demonstrating the efficacy of transplantation therapy using ES cell–derived DA neurons in an experimental primate model of PD.

Results

Induction of neural progenitors from monkey ES cells. To enrich graftable neural progenitors, we first cultured monkey ES cells on PA6 stromal feeder cells, then detached the cells from the feeders for

Nonstandard abbreviations used: ChAT, choline acetyltransferase; DA, dopaminergic; DAT, dopamine transporter; GABA, γ-amino butyric acid; GalC, galactocerebroside C; GFAP, glial fibrillary acidic protein; GMEM, Glasgow minimum essential medium; i.m., intramuscular(ly); LIF, leukemia inhibitory factor; ME, mercaptoethanol; MPTP, 1-methyl-4-phenyl-1,2,3,6-tetrahydropyridine; NCAM, N cell adhesion molecule; OL, poly-l-ornithine and laminin; PD, Parkinson disease; PET, positron emission tomography; SDIA, stromal cell–derived inducing activity; TH, tyrosine hydroxylase.

Conflict of interest: The authors have declared that no conflict of interest exists.

Citation for this article: *J. Clin. Invest.* 115:102–109 (2005). doi:10.1172/JCI200521137.

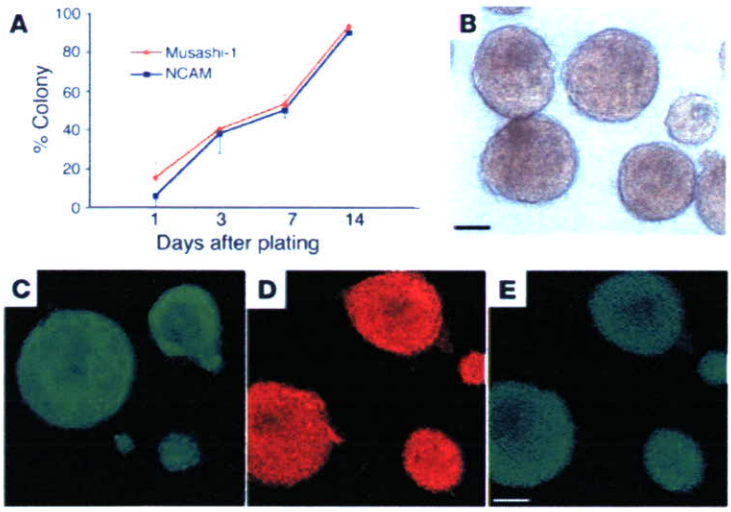

Figure 1
Neural progenitors induced from primate ES cells. (**A**) Time course of neural progenitor marker expression in monkey ES cells cultured on PA6 cells. (**B**) Detached ES cell colonies formed spheres similar to those of neural progenitor cells. (**C–E**) Spheres were immunoreactive for NCAM (**C**, green), Musashi-1 (**D**, red), and Nestin (**E**, green). Scale bar: 100 μm.

expansion as neurospheres. ES cells began to differentiate on PA6 cells, with cells immunoreactive for neural progenitor markers, such as N cell adhesion molecule (NCAM) and Musashi-1 (11, 14), emerging within three days. ES cells proliferated and differentiated on the feeder layer by forming colonies, and cells positive for neural markers increased in number until 2 weeks into the culture period. The percentages of the colonies including at least 1 NCAM- or Musashi-1–positive cell reached approximately 100% at 2 weeks of culture (NCAM = 90.4% ± 7.5%, Musashi-1 = 97.5% ± 4.6%, n = 100 from 3 independent cultures; Figure 1A). At this time point, 78.3% ± 7.5% of the total cells were immunoreactive for NCAM, 75.0% ± 15.4% for Musashi-1, and 72.3% ± 9.1% for another neural progenitor marker, Nestin (14). These results indicate that the majority of the ES cells were committed to the neural lineage by day 14 of culture on feeder layers.

In vitro characterization of neural progenitors derived from monkey ES cells. To further enrich neural progenitors, we detached the ES cells from the feeder layer on day 14, then continued to culture the cells on noncoated dishes in serum-free medium containing FGF2, EGF, and leukemia inhibitory factor (LIF). During the next few days, the cells formed spheres morphologically resembling those formed by neural progenitor cells (Figure 1B). These spheres were positively stained with antibodies specific for neural progenitor cell markers NCAM, Musashi-1, and Nestin (Figure 1, C–E). To determine the potential of these cells to differentiate, we expanded the cells as spheres for 7 days, then induced differentiation by culturing the cells on poly-l-ornithine and laminin–coated (OL-coated) slides for 7 days. We removed the mitogens FGF2, EGF, and LIF from the medium, instead adding neurotrophic factors such as brain-derived neurotrophic factor and neurotrophin-3. Immunofluorescence analysis revealed that the cells differentiated into mature neural cells expressing the neuronal markers TuJ1 (52.8% ± 16.0% of DAPI) and Map2ab (38.3% ± 7.5% of DAPI), the astroglial marker glial fibrillary acidic protein (GFAP) (28.6% ± 17.6% of DAPI), and the oligodendroglial marker galactocerebroside C (GalC) (0.6% ± 0.4% of DAPI) (Figure 2, A–D and I). Further analyses demonstrated that these neurons derived from ES cells were immunoreactive for γ-amino butyric acid (GABA) (28.6% ± 10.7% of TuJ1), glutamate (14.3% ± 5.3% of TuJ1), choline acetyltransferase (ChAT) (0.7% ± 0.3% of TuJ1), and serotonin (3.3% ± 1.7% of TuJ1) (Figure 2, E–H and J). These results suggest that ES cell–derived spheres contain neural progenitor cells.

Effect of growth factors on differentiation of DA neurons. Effective treatment of PD requires substantial quantities of DA neurons. The percentage of tyrosine hydroxylase–positive (TH-positive) cells derived from neurospheres was only 5.4% ± 1.8% of the TuJ1-positive cells (Figure 2J). To increase the percentage of these cells, we examined the effects of various combinations of growth factors on neurosphere culture. The percentage of

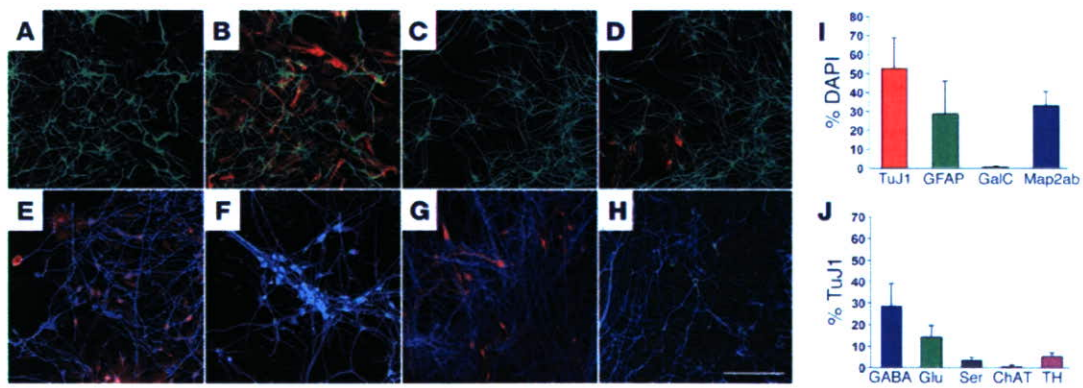

Figure 2
Expression of differentiated neural and neuronal subtype markers. Differentiated spheres were stained with antibodies against TuJ1 (**A** and **B**, green; **E–H**, blue), GFAP (**B**, red), Map2ab (**C** and **D**, green), GalC (**D**, red), GABA (**E**, red), glutamate (Glu; **F**, green), serotonin (Ser; **G**, red), and ChAT (**H**, green). Scale bar: 100 μm. The proportions of cells expressing differentiated neural (**I**) and neurotransmitter-related (**J**) markers are expressed as the mean ± SD of 3 independent cultures.

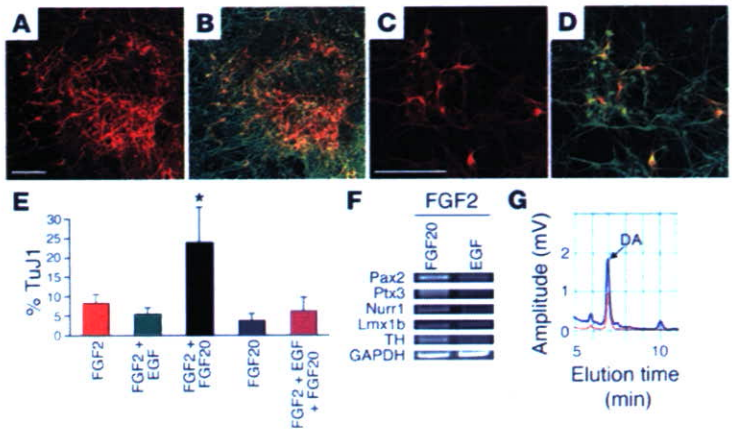

Figure 3
DA neurons differentiated from ES cell–derived neurospheres. (**A–D**) Differentiated spheres treated with FGF2 and FGF20 were stained with antibodies against TH (red) and TuJ1 (green). Scale bars: 50 μm. (**E**) The proportion of TH-positive cells to TuJ1-positive cells is expressed as the mean ± SD of 3 to 5 independent cultures. *$P < 0.05$. (**F**) RT-PCR for mesencephalic DA neuron markers *Pax2*, *Ptx3*, *Nurr1*, *Lmx1b*, and *TH* in cells treated with FGF2 and FGF20 (left) or FGF2 and EGF (right). (**G**) HPLC measuring concentration of dopamine released by SDIA- and FGF2- and FGF20-treated monkey ES cells in response to high K^+ depolarizing stimuli (blue line). Dopamine standard, red line.

TH-positive neurons out of total Tuj1-positive cells increased to 24% in the presence of FGF2 and FGF20 (Figure 3, A–E). Neither FGF2 nor FGF20 alone caused an increase in the number of TH-positive neurons. In the presence of FGF2, however, FGF20 increased the rate of TH differentiation in a dose-dependent manner (1 pg/ml = 3.8% ± 1.8% of TuJ1, 10 pg/ml = 8.8% ± 4.8% of TuJ1, 1 ng/ml = 24.3% ± 9.8% of TuJ1).

RT-PCR analyses showed that the cells derived from SDIA-induced neurospheres expressed mesencephalic DA neuron markers such as *Pax2*, *Ptx3*, *Nurr1*, *Lmx1b*, and *TH* (15, 16). The expression of these markers was more abundant in FGF2- and FGF20-treated cells than in FGF2- and EGF-treated cells (Figure 3F). Furthermore, FGF2- and FGF20-treated cells released 55.6 ± 19.9 pmol per 10^6 cells of dopamine in response to high K^+ depolarizing stimuli as assayed by HPLC ($n = 5$; Figure 3G). These results indicate that monkey ES spheres treated both with SDIA and with FGF2 and FGF20 generate a significant number of functional DA neurons in vitro.

Transplantation of DA neurons from ES-derived neural progenitors. To determine if the isolated TH-positive neurons function as DA neurons in vivo, ES cell–derived neurospheres were grafted into the putamen of the monkeys with MPTP-induced PD. In this primate model of PD, we administered MPTP intravenously to *Macaca fascicularis* (cynomolgus monkeys), hereafter *M. fascicularis*, and evaluated their behavior by scoring for neurological symptoms, such as motility and tremor (Table 1). Only the animals that exhibited stable deterioration for periods longer than 12 weeks were used for transplantation. ES cell–derived neurospheres used for grafting were prepared by treating with SDIA for 14 days and, subsequently, with FGF2 and FGF20 for 7 days, as described above. Using MRI images obtained for each monkey, we determined the necessary coordinates to stereotactically transplant the cells (300,000–600,000 cells per side) into the bilateral putamen. After injection, we continuously analyzed the behavior of postoperative monkeys by assessing neurological scores. We observed a slight recovery in the behavioral symptoms even in the sham-operated animals. At 10 weeks after transplantation, however, the mean scores of ES cell–transplanted monkeys significantly improved over the levels observed in sham-operated ones (Figure 4A, $n = 6$ and 4, respectively). In our evaluation of symptoms after transplantation, posture recovery was the most prominent improvement seen in ES cell–transplanted monkeys, with significant improvements in motility also observed. There were, however, no significant changes in head-checking movement. Consciousness was not disturbed in any preoperative animals, and no deterioration was observed postoperatively. In addition, none of the treated animals developed dyskinesia. Positron emission tomography (PET) at 14 weeks after transplantation revealed increases in ^{18}F-fluorodopa uptake at the putamen of the ES cell–transplanted animals (Figure 4, B and C).

After the PET study, animals were sacrificed and subjected to immunohistochemical analysis. Grafted cells, which were labeled by BrdU treatment during sphere culture, were detected in the putamen of ES cell–transplanted monkeys (7,996 ± 3,300 cells per side; Figure 5, A–C). DA neurons were detected by TH (Figure 5, B, C, E, and F; ref. 11) or dopamine transporter (DAT) (Figure 5, H and I; ref. 17) staining. An average of 2130 ± 645 TH-positive cells per side survived. Double labeling immunofluorescence microscopy revealed that 65.5% ± 4.3% and 50.3% ± 6.1% of the TH- and DAT-positive cells were immunoreactive for BrdU, respectively. Thus, the estimated number of TH/BrdU–double-positive cells was 1395 per side, 17.4% of the total of BrdU-positive cells. In contrast, in sham-operated monkeys, only a few TH-positive cells and scattered fibers were detectable in the putamen. No tumor formation or Ki-67–inducing reactivity was observed. As for other

Table 1
Neurological scores of MPTP-treated monkeys

Behavior	Scores
Alertness	Normal, 0; reduced, 1; absent, 2
Head-checking movement	Present, 0; reduced, 1; absent, 2
Eyes	Normal, 0; reduced blinking, 1; eyes closed, 2
Posture	Normal, 0; mildly abnormal, 1; abnormal, 2; grossly abnormal, 3
Balance	Normal, 0; impaired, 1; frequent falling, 2; no movement, 3
Motility, at rest	Normal, 0; mild bradykinesia, 1; bradykinesia, 2; akinesia, 3
Motility, reaction to external stimuli	Normal, 0; mildly reduced, 1; reduced, 2; absent, 3
Walking	Normal, 0; mildly reduced, 1; reduced, 2; no walking, 3
Tremor	Absent, 0; mild/not always, 1; moderate, 2; severe, 3

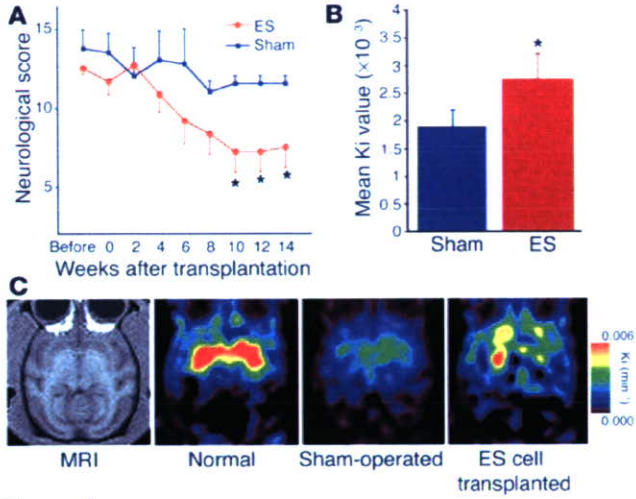

Figure 4
Function of ES cell–derived neurospheres in MPTP-treated monkeys. Behavioral scores (**A**) and PET study (**B** and **C**) of ES cell–transplanted ($n = 6$) and sham-operated animals ($n = 4$). (**B**) Mean Ki values from entire putamen. (**C**) Increased ^{18}F-fluorodopa uptake in the putamen of ES cell–transplanted animals. All values are mean ± SD. *$P < 0.05$.

neuronal phenotypes, GABA-positive cells were detected in the graft at a slightly higher frequency than TH-positive cells, while few serotonin-positive cells were present (data not shown).

Discussion

Following initial work by Thomson et al. reporting a method for establishing primate ES cells (18), Suemori et al. (19) recently devised a similar scheme for generating *M. fascicularis* ES cells. Lee et al. recently reported a 5-step method to induce DA neurons from ES cells through the induction of neural progenitor cells from embryoid bodies (20). Transplantation of induced DA neurons derived from mouse ES cells improves the neurological symptoms of rats with a Parkinson-like syndrome induced by treatment with 6-hydroxydopamine (6-OHDA) (21). We have also reported a method of inducing DA neurons based on SDIA resulting from coculture of ES cells on a PA6 stromal feeder layer. By the use of this method, mouse ES cells are diverted to a neuronal fate with TH-positive DA neurons composing 30% of total TuJ1-positive neurons (10). Furthermore, this method produced similar results with *M. fascicularis* ES cells (11). In this study, we produced a highly enriched population of proliferating neural progenitors derived from SDIA-treated monkey ES cells. Furthermore, treatment of these cells with a combination of FGF2 and FGF20 induced the generation of a large population of DA neurons from ES cell–derived neural progenitors. Using MPTP-treated monkeys as a primate model for PD, we analyzed the effect of administration of DA neurons generated from monkey ES cells in vivo. Behavioral studies and functional imaging revealed that the transplanted cells functioned as DA neurons, attenuating the MPTP-induced symptoms.

In our preparation of graftable cells, we made two major modifications to our previously published protocol (10, 22). First, we induced the formation of neurospheres, expecting an enrichment of neuronal progenitor cells. We detached the ES cells from the feeder layer on day 14 and cultured them on noncoated dishes. Under these conditions, the cells formed floating spheres composed of neural precursor cells. Since the serum-free culture medium was suitable for neural cell growth, any contaminating nonneural and PA6 cells were likely eliminated as a result of a low proliferation rate and/or adherence to the bottom of the dish. Our previous report (22) demonstrated that, when grafted into the brain, fully maturated TH-positive neurons survived less efficiently than DA neuron progenitors induced by SDIA, probably due to their susceptibility to mechanical stress. This result is consistent with the fact that transplantation of mesencephalon tissues from early gestation stage embryos undergoing neurogenesis of DA neurons resulted in good survival of TH-positive cells (1300–18,000) and increased dopamine concentrations in the caudate nucleus of MPTP-treated monkeys, whereas these effects are not observed when mesencephalon tissues from later stages are transplanted (23). Thus, ES cell–derived neuronal progenitors competent to generate DA neurons appear to be more suitable for transplantation than DA neurons matured in vitro.

Another important modification to our previous protocol is the use of FGF2 and FGF20 treatment to enhance the generation of DA neurons. The percentage of TH-positive neurons generated from

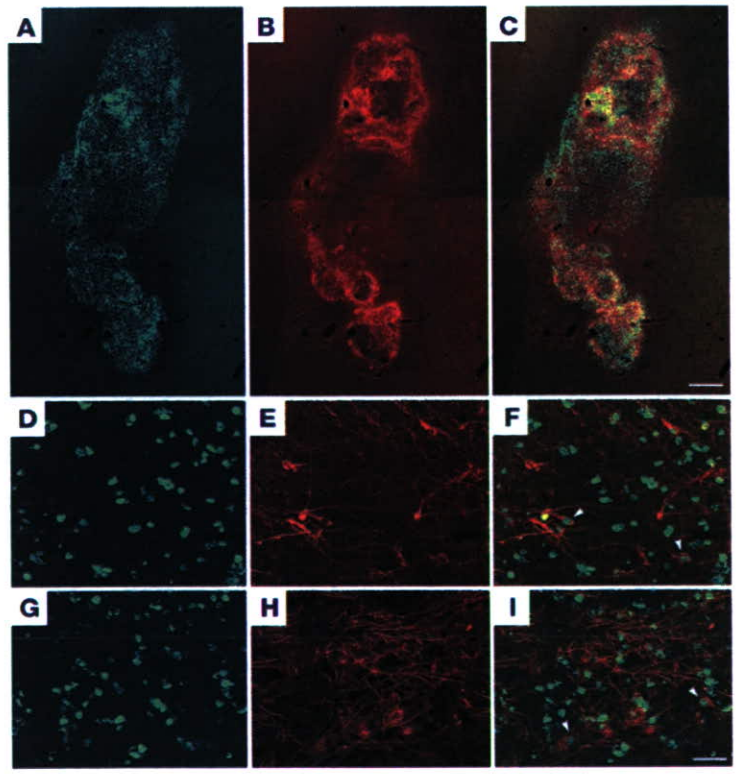

Figure 5
Survival of ES cell–derived DA neurons in the striatum. (**A–C**) Grafted cells (BrdU-labeled, green) survived and differentiated into DA neurons (TH-positive, red) along the needle tract (merged image **C**). Scale bar: 500 μm. (**D–I**) Colocalization (arrows in **F** and **I**) of BrdU (**D**, **F**, **G**, and **I**, green) and TH (**E** and **F**, red) or DAT (**H** and **I**, red) shows that graft-derived cells have dopaminergic character. Scale bar: 50 μm.

neurospheres was 5.4 ± 1.8% of TuJ1, much lower than that generated by culturing on PA6 cells (35%; ref. 10). This discrepancy most likely results from mechanical damage caused by detaching the cells or inappropriate culture conditions for spheres. To increase the number of DA neurons differentiated from neurospheres, we examined the effects of various additional growth factors. Ascorbic acid and Sonic hedgehog, which were used in the 5-step method (20), did not increase the proportion of TH-positive cells (data not shown). In contrast, FGF20 treatment in combination with FGF2 was able to efficiently increase the proportion of TH-positive cells. FGF20 is a secreted protein that is preferentially expressed in the substantia nigra pars compacta of the rat brain (13). The expression profile of FGF20 is quite different from that of other FGF family members, which suggests that FGF20 plays a unique role in the brain. Furthermore, recombinant FGF20 enhances the survival of primary DA neurons (13). FGF receptor-1c, the receptor through which FGF20 activates the mitogen-activated protein kinase pathway, is also preferentially expressed in the substantia nigra pars compacta (24). Our results raise the possibility that FGF20 in combination with FGF2 may support the survival or promote the proliferation of progenitors of DA neurons, resulting in the enrichment of DA progenitor cells in spheres. The mechanism by which this combined stimulation of FGF2 and FGF20 facilitates the production of DA neurons remains to be clarified.

FGF2 and EGF are reported to play different roles in the differentiation of neural precursors. Although FGF2 and EGF promote proliferation of neural precursor cells, the former promotes neuronal differentiation, while the latter induces glial differentiation (12, 25, 26). They also have different effects on the differentiation of embryoid bodies derived from human ES cells (27). In the present study using neural precursors derived from primate ES cells, FGF2 increased differentiation of ES cells into DA neurons, while EGF suppressed this process even in the presence of FGF2 and FGF20. It is possible that EGF interferes with the differentiation of SDIA-treated spheres into DA neurons directly or indirectly by promoting astroglial induction. Alternatively, EGF may stimulate proliferation or differentiation of a different cell population than that stimulated by FGF2. The differential effects of growth factors present an intriguing topic for future investigation.

In primate studies, functional neuroimaging is a useful tool for in vivo assessment of differentiation, survival, and functional integration of grafted cells. PET imaging of presynaptic targeting reagents such as fluoro-dopa, fluoro-metatyrosine, or 2β-carbomethoxy-3β-4-fluorophenyltropane (CFT) determines whether cells implanted in vivo have the molecular machinery necessary for dopamine synthesis and/or storage (28–30). In this study, we examined the uptake of fluoro-dopa at 14 weeks after transplantation. The significant increase in the mean Ki value in the putamen of ES cell–transplanted animals indicated that the grafted cells functioned as DA neurons. A postmortem examination of the ES cell–transplanted monkey in Figure 4C revealed that more TH-positive cells survived within the right putamen. This finding reflects the correlation of the PET results with the survival of DA neurons. For future studies, detailed analyses using additional tracers, including postsynaptic markers such as fluoro-raclopride, should allow for further understanding of the functional aspects of grafted cells. In this study, we detected significant differences in the mean Ki values from the entire putamen between the ES cell–transplanted monkeys and the sham-treated control monkeys 3 months after surgery. Widner et al. (8) reported that striatal uptake of fluoro-dopa was unchanged 5 to 6 months postoperatively, but increased markedly at 12 to 13 and 22 to 24 months in patients who received fetal mesencephalic grafts. Freed et al. (4) reported an improved Ki value from the entire putamen 6 months after transplantation. Given the lengthier monitoring periods in these reports, our evaluation of mean Ki values at 3 months may still be premature; further PET studies at later time points may result in even greater changes.

MPTP is a neurotoxin that causes selective destruction of DA neurons in the substantia nigra pars compacta, inducing PD-like symptoms in primates (31, 32). Following repetitive intravenous injections of MPTP (approximately 17 mg in total per animal), monkeys stably exhibited PD-like symptoms more than 12 weeks before transplantation surgery. With a blind evaluation based on neurological scores, we detected significant behavioral improvements in the ES cell–transplanted monkeys 10 weeks after transplantation. Recently, 2 double-blind placebo-controlled clinical trials of fetal nigral transplantation (4, 7) demonstrated that younger patients and patients with mild symptoms improved after treatment, with behavioral recovery first observed in the 3 to 4 month period following surgery. In this study, posture and motility were the symptoms showing the most marked improvement. These results are comparable with clinical reports (4, 33) demonstrating improvements in rigidity and hypokinesia.

PET and immunofluorescence studies demonstrated that a substantial number of the grafted cells survived in the putamen to function as DA neurons. We transplanted 300,000–600,000 cells into each side of the brain in each monkey. The number of surviving cells detected by BrdU staining was approximately 8,000 per side. Thus, the survival rate of the grafted cells was 1.3% to 2.7%, although the actual value could be higher (discussed below). Through TH staining, the number of surviving DA neurons was shown to be approximately 4,300 per brain. In normal brains, there are no DA neuron cell bodies in the striatum, only fibers. Thus, these TH-positive cells were considered to be derived from the grafted ES cells. While the grafted cells were labeled by BrdU prior to transplantation, only 65% of these TH-positive cells were immunoreactive for BrdU. This may have resulted from incomplete labeling of the input cells; as the cells were treated with BrdU while being cultured as spheres, the labeling rate was not 100%, but 68.8%. In addition, grafted cells might proliferate in vivo, reducing the concentration of BrdU in the cells. Furthermore, intrinsic striatal TH-positive neurons may be recruited, as reported previously (34), which may explain the observation of a few TH-positive neurons even in control monkeys.

According to an earlier clinical report, the number of TH-positive cells in the postmortem brain of a PD patient was approximately 200,000 (35). In 2 recent double-blind trials, however, the number of surviving TH-positive cells was determined to be 50,000–240,000 (4, 7). Given that the volume of the monkey putamen is 10% of that of the human putamen (36, 37), it is likely that the required number of TH-positive cells in the monkey (*M. fascicularis*) brain is 5,000–24,000. The results of this study remain in keeping with observations made in human patients, suggesting that ES cells are a promising candidate for a donor source for cell transplantation treatment of PD. It should be noted, however, that the MPTP-treated monkey is a model of acute selective nigral destruction whereas human PD patients also experience progressive deterioration and pathological changes of other neural systems (15, 38, 39).

Although the results presented here encourage the development of strategies involving ES cell–derived neurons for treatment of neurological diseases, further studies will be needed to address the long-term efficacy and safety of using these cells. For instance, the low survival rate of the grafted cells or neurons is comparable to that noted in previous reports (40). To increase the number of viable DA neurons produced by grafts in vivo, we used DA neuron progenitors in the present study. Multiple-target grafting (41) is also a strategy that should be considered. Notably, we observed a number of GABA-positive cells in the graft, suggesting that other types of neurons and/or glial cells in the graft may contribute to both the differentiation and function of transplanted DA neurons (42). However, the optimal cellular composition of the graft remains to be determined. In addition, while previous studies with rodents have demonstrated that tumor formation can be associated with ES cell grafts (43–45), we did not observe tumor formation or Ki67-positive cells within the first 3 months after transplantation. In the future, however, it will be important to examine late tumor formation as well as the possible long-term effects of ES cell grafts on motor behavior. It will also be necessary to use non–TH-positive cells in control grafts to exclude the possibility that the effects of this treatment are mediated by non-DA cells.

Finally, we would like to emphasize that our system (MRI, surgery, PET, etc.) is applicable to humans. Previous work has shown that monkey ES cells have characteristics similar to those of human ES cells (18, 19, 46). In addition, it was recently demonstrated that neural precursors induced from human ES cells were able to survive in rodent brains (47, 48). The SDIA method is applicable to human ES cells, allowing for enrichment of DA progenitors (unpublished data). These results suggest that transplantation using ES cells as a clinical therapy for PD is approaching the point of technical feasibility. Two recent double-blind, sham surgery–controlled trials of embryonic mesencephalic transplants for the treatment of PD, however, showed only modest improvement (4, 7), suggesting the potential limits of cell transplantation. Many basic issues, especially regarding stem cell therapy, remain to be resolved (38). Before the clinical application of human ES cell transplantation can be attempted, extensive studies assessing the safety and efficacy of ES cell transplantation in monkey models will be necessary.

Methods

Maintenance of primate ES cells. Cynomolgus monkey ES cell lines were established and their pluripotency confirmed by teratoma formation in mice with severe combined immunodeficiency, as previously described (19). Undifferentiated ES cells were maintained on a feeder layer (i.e., STO) of embryonic fibroblasts treated with mitomycin C (Wako Pure Chemical Industries Ltd.) in DMEM (Sigma-Aldrich)/F-12 (Invitrogen Corp.) supplemented with 0.1 mM 2-mercaptoethanol (2-ME) (Sigma-Aldrich), 1,000 units/ml LIF (Chemicon International), 20% knockout serum replacement (KSR; Invitrogen Corp.), and 4 ng/ml FGF2 (Upstate Biotechnology Inc.). ES cells were subcultured using 0.25% trypsin (Invitrogen Corp.) in PBS with 20% KSR and 1 mM $CaCl_2$ (Wako Pure Chemical Industries Ltd.) as described (11, 19).

Induction of neural progenitors from primate ES cells. PA6 cells plated on type I collagen-coated chamber slides (BD) or gelatin-coated dishes (gelatin from Sigma-Aldrich; dishes from BD) were used as a feeder cell layer. To avoid contamination by incidentally differentiating cells, we manually selected undifferentiated ES cell colonies with stem cell–like morphology (tightly packed cells exhibiting a high nucleus to cytoplasm ratio). Undifferentiated ES cell colonies were washed twice with Glasgow minimum essential medium (GMEM) (Sigma-Aldrich) supplemented with 10% KSR, 1 mM pyruvate (Sigma-Aldrich), 0.1 μM nonessential amino acids, and 0.1 mM 2-ME. After trypsinization, partially dissociated ES cell clumps (10–50 cells per clump) were plated on PA6 cells at 1000 clumps per 10-cm dish. Cells were then cultured in GMEM supplemented with 5% KSR, 2 mM glutamine, 0.1 mM nonessential amino acids, 1 mM pyruvate, and 0.1 mM 2-ME for 2 weeks. Differentiated colonies were detached from feeder cells using a papain dissociation system (Worthington Biochemical Corp.). Isolated colonies were cultured in neurobasal medium (Invitrogen Corp.) supplemented with B27 supplement (Invitrogen Corp.), 20 ng/ml FGF2, and 20 ng/ml EGF (R&D Systems) for 1 week. In the experiments examining the effects of growth factors on neurosphere culture, the indicated concentrations of FGF20 (1pg/ml, 10 pg/ml and 1 ng/ml) were added to medium with or without FGF2 and EGF. In order to evaluate the expression of neural progenitor cell markers by each cell, spheres were incubated with papain at 37°C for 10 minutes and then mechanically dissociated into single cells. After incubation with a papain inhibitor, the dissociated cells were plated on OL-coated slides (OL from Sigma-Aldrich) at a density of 10^5 cells/cm^2. After 16 hours, they were fixed in 4% paraformaldehyde (Sigma-Aldrich) and evaluated by immunofluorescence.

Differentiation of neural progenitor cells. Spheres were isolated manually and plated on OL-coated slides in neurobasal medium to which had been added B27 supplement, 20 ng/ml brain-derived neurotrophic factor (Sigma-Aldrich), and 20 ng/ml neurotrophin-3 (Sigma-Aldrich). After 1 week of culture, spheres were fixed or used for additional experiments.

RT-PCR analysis. Total RNA was isolated from differentiated cells using a TRIzol kit (Invitrogen Corp.) according to the manufacturer's instructions. cDNA synthesis was carried out using the SuperScript Double Stranded cDNA Synthesis kit (Invitrogen Corp.). PCR was performed using KOD-plus polymerase (Toyobo Co.), with the following cycling conditions: 30 seconds at 94°C, 30 seconds at 60.5°C, 60 seconds at 68°C × 30 cycles for Pax2, Ptx3, Nurr1, and GAPDH; and 30 seconds at 94°C, 30 seconds at 66°C, 60 seconds at 68°C × 30 cycles for Lmx1b and TH in a thermal cycler (Astec Co.). The experiments were repeated 4 to 7 times for confirmation, and PCR products were sequenced to rule out false positives. The primers used are as follows: *Pax2*, TGTGTCAGCAAAATCCTGGGCAGGT and TGCTGAACTTTGGTCCGGATGAT; *Ptx3*, TTCGCCTTCAACTCGGTCAACGT and CCCAGGGTCTGAAAGGGGTG; *Nurr1*, CTCCCAGAGGGAACTGCACTTCG and CTCTGGAGTTAAGAAATCGGAGCTG; *Lmx1b*, GCAGCGGCTGCATGGAGAAGATCGC and GGTTCTGAAACCAGACCTGGACCAC; *TH*, GACTGCTGCCACGAGCTGCTGGG and TCTTGGTAGGGCTGCACGG; and *GAPDH*, GTGAAGGTCGGAGTCAACG and GGTGAAGACGCCAGTGGACTC.

Dopamine release assay. Spheres treated with FGF2 and FGF20 were plated onto 35mm OL-coated dishes at a density of 50 spheres per dish and made to differentiate for 1 week. Then, after being rinsed in a low-KCl (4.7 mM) solution, the cells were incubated in 1 ml of a high-KCl solution (20 mM HEPES-NaOH, pH 7.4, 85 mM NaCl, 60 mM KCl, 2.5 mM $CaCl_2$, 1.2 mM $MgSO_4$, 1.2 mM KH_2PO_4, and 11 mM glucose) for 15 minutes. Concentrations of dopamine were determined by HPLC using a reverse-phase column and an electrochemical detector system (HTEC 500; Eicom Corp.) as previously described (49).

Animal model. Adult male cynomolgus monkeys (*M. fascicularis*) weighing 2.5–3.5 kg were given intravenous injections of MPTP HCl (0.4 mg/kg as free base, Sigma-Aldrich) twice a week until persistent Parkinsonian behavioral disturbances, such as tremor, bradykinesia, and impaired balance, became evident. Animals were given an average of 14.7 MPTP shots and exhibited stable Parkinsonism for approximately 30 days. To prevent any possibility of spontaneous recovery, only those monkeys that presented

stable deterioration for a period greater than 12 weeks were used for transplantation experiments. All animals were fed with commercial pellets and fresh fruits and had free access to clean water. Monkeys were cared for and handled according to Guidelines for Animal Experiments of Kyoto University and the National Cardiovascular Center (Osaka, Japan) and the Guide for the Care and Use of Laboratory Animals from the Institute of Laboratory Animal Resources (ILAR; Washington, DC, USA).

MRI. For accurate orientation of the putamen, animals (n = 10; 6 for ES transplanted and 4 for sham-operated group) were subjected to MRI examination using a 3.0 Tesla Signa system (General Electric). Following anesthesia by intramuscular injection with ketamine hydrochloride (15 mg/kg; Sankyo Co.) and xylazine (1.5 mg/kg; Boehringer Ingelheim Vetmedica Inc.), animals were positioned into the magnet using an MR-compatible headholder. T1-weighted images were used for further examination.

Transplantation. Following anesthesia with pentobarbital (7.5 mg/kg, intramuscularly [i.m.]; Dainippon Pharmaceutical Co.) and ketamine (10 mg/kg, i.m.), monkeys were fixed in a surgical frame (Narishige SN-1N; Narishige Co.). Neural progenitors from monkey ES cell cultures in two 6-cm dishes (300,000–600,000 cells per dish) were collected for each animal. While the ES cells were expanding as spheres, BrdU (5 μg/ml; Sigma-Aldrich) was added to the culture medium for 7 days to label the ES cells. Using an electric injector (Muromachi Kikai Co.), we transplanted donor cells into the putamen bilaterally, using the MRI findings for each monkey and the *M. fascicularis* brain atlas (36, 50). To cover the mid to posterior putamen, 3 targets that were 2 mm apart in anterior-posterior position and 1–2 mm in medial-lateral position were set, and 4 injections (1 μl/60 seconds for each injection) were made along each tract. After surgery, all animals were given antibiotics for 1 week and a daily immunosuppressant (cyclosporin A, 10 mg/kg, i.m.; Carbiochem) until sacrifice. Monthly blood analyses performed over the course of the experiment confirmed the levels of circulating cyclosporin A, which averaged 393 ng/ml. In control monkeys undergoing sham operations, the equivalent volume of culture medium was administered without cells. Afterward, antibiotics and immunosuppressants were injected as for the cell-grafted monkeys.

Immunofluoresence study. For in vitro studies, cells were fixed in 4% paraformaldehyde for 10 minutes for microscopic observation. For in vivo studies, after administration of deep anesthesia with pentobarbital and ketamine, monkeys (n = 10; 6 for ES cell–transplanted and 4 for sham-operated group) were transcardially perfused with 4% paraformaldehyde. Excised brains were frozen and cut with a microtome at a 50-μm thickness. Sections were then stained by the free-floating method. Slides were first incubated in 0.3% Triton X with 5% skim milk in PBS for 30 minutes. Samples were then incubated with one of the following primary antibodies: rabbit anti-NCAM (1:300; Chemicon Inc.), rat anti–Musashi-1 (1:200; gift from H. Okano, Keio University, Japan), mouse anti-Nestin (1:300; Chemicon Inc.), mouse anti-TuJ1 (1:300; BabCO), rabbit anti-GFAP (1:1000; Chemicon Inc.), mouse anti-Map2ab (1:250; Sigma-Aldrich), rabbit anti-GalC (1:100; Chemicon Inc.), rabbit anti-glutamate (1:200; Chemicon Inc.), goat anti-ChAT (1:1000; Chemicon Inc.), mouse anti-GABA (1:1000; Sigma-Aldrich), mouse anti-BrdU (1:200; BD), rabbit anti-TH (1:60; Chemicon Inc.), rabbit anti-serotonin (1:2000; DiaSorin Inc.), or rat anti-DAT (1:100; Chemicon Inc.) in 2% skim milk in PBS overnight at 4°C. After 3 washes in PBS, samples were incubated with the appropriate secondary antibodies for 1 hour at room temperature: FITC-labeled anti-mouse Ig (1:200; Jackson Immunoresearch Laboratories Inc.) and Cy3-labeled anti-rabbit Ig (1:200; Jackson Immunoresearch Laboratories Inc.). For nuclear staining, 200 ng/ml of 4′,6′-diamidino-2-phenylindole (DAPI) was added in the final wash. After being washed in PBS, samples were mounted and analyzed using a Fluoview FV300 laser confocal microscope (Olympus Optical Co.). For in vitro studies, cells in 5 randomly selected fields, each of which included 100–500 cells, were counted for 3 to 5 independent cultures. For in vivo studies, the number of immunoreactive cells was quantified in every sixth section throughout the graft and surrounding tissue. Statistical analysis was performed by one-way ANOVA and post hoc multiple comparison by the Dunn test. A P value of less than 0.05 was considered significant.

Behavioral assessment. Parkinsonian behavior was evaluated using a rating scale previously proposed by Akai et al. (51), with modifications (Table 1). To prevent subjective biases, the evaluation was performed by a trained examiner who was not involved in the culturing and transplantation of the cells and not informed of the specific procedure to which each monkey was subjected. Student's t test was used to compare the 2 groups, and a P value of less than 0.05 was considered significant.

PET. To evaluate the in vivo DA function of the grafted cells, PET scans using ^{18}F-fluorodopa were performed on each animal prior to perfusion. Under generalized anesthesia with a continuous infusion of propofol (4 mg/kg/h; Zeneca Pharmaceuticals) and vecuronium-bromide (0.25 mg/kg/h; Boehringer Ingelheim Vetmedica Inc.), analyses were performed using an ECAT EXACT HR+ PET scanner (Siemens/CTI). After intravenous injection of 185MBq of ^{18}F-fluorodopa, brain radioactivity was assessed for 90 minutes in animals that had received carbidopa (10 mg/kg) 30 minutes prior to the PET scan. Parametric images of the dopamine-irreversible metabolic rate of Ki (min^{-1}), considered to be a measure of presynaptic DA function, were generated using the time course of radioactivity in each voxel by multiple-time graphical analysis (52) using the bilateral occipital lobes as a reference region. The ^{18}F-fluorodopa Ki image was coregistered to the corresponding T1-weighted MRI image, which was obtained by an inversion-recovery prepared fast spoiled gradient recalled acquisition in the steady state (IR-FSPGR) sequence (Tr = 9.4, TI = 600, TE = 2.1 in msec) using a 3.0 Tesla Signa System (General Electric) and realigned to a standard space of *M. fascicularis* (36, 50). DA function was evaluated by visual inspection of Ki images and by quantitative Ki values in the bilateral striatum identified by the corresponding MRI image. This evaluation was performed in a blind manner to ensure objectivity. Student's t test was used to compare the results.

Acknowledgments

The authors thank H. Sameshima and T. Yamamoto (Shin Nippon Biomedical Laboratories Ltd.) for technical help with monkeys, H. Okano (Keio University) for kindly providing the Musashi-1 antibody, and Hiroyuki Nawa (Niigata University) for helpful advice regarding the dopamine release assay. We also thank Y. Yanagi and T. Gomibuchi for their secretarial help. This study was supported by the following: Grants-in-Aid for Scientific Research, Grants in Kobe Knowledge Cluster, and Establishment of International Center of Excellence for Integration of Transplantation Therapy and Regenerative Medicine from the Ministry of Education, Culture, Sports, Science and Technology; Health Sciences Research Grants in Research on Human Genome, Tissue Engineering and Food Biotechnology from the Ministry of Health, Labour and Welfare; and Grants in Organization for Pharmaceutical Safety and Research.

Received for publication January 22, 2004, and accepted in revised form November 2, 2004.

Address correspondence to: Jun Takahashi, Department of Neurosurgery, Kyoto University Graduate School of Medicine, 54 Kawahara-cho, Shogoin, Sakyo, Kyoto 606-8507, Japan. Phone: 81-75-751-3450; Fax: 81-75-752-9501; E-mail: jbtaka@kuhp.kyoto-u.ac.jp.

1. Bergman, H., and Deuschl, G. 2002. Pathophysiology of Parkinson's disease: from clinical neurology to basic neuroscience and back. *Mov. Disord.* **17**(Suppl. 3):S28–S40.
2. Dostrovsky, J.O., Hutchison, W.D., and Lozano, A.M. 2002. The globus pallidus, deep brain stimulation, and Parkinson's disease. *Neuroscientist.* **8**:284–290.
3. Miyasaki, J.M., Martin, W., Suchowersky, O., Weiner, W.J., and Lang, A.E. 2002. Practice parameter: initiation of treatment for Parkinson's disease: an evidence-based review: report of the Quality Standards Subcommittee of the American Academy of Neurology. *Neurology.* **58**:11–17.
4. Freed, C.R., et al. 2001. Transplantation of embryonic dopamine neurons for severe Parkinson's disease. *N. Engl. J. Med.* **344**:710–719.
5. Hagell, P., and Brundin, P. 2001. Cell survival and clinical outcome following intrastriatal transplantation in Parkinson disease. *J. Neuropathol. Exp. Neurol.* **60**:741–752.
6. Lindvall, O., et al. 1994. Evidence for long-term survival and function of dopaminergic grafts in progressive Parkinson's disease. *Ann. Neurol.* **35**:172–180.
7. Olanow, C.W., et al. 2003. A double-blind controlled trial of bilateral fetal nigral transplantation in Parkinson's disease. *Ann. Neurol.* **54**:403–414.
8. Widner, H., et al. 1992. Bilateral fetal mesencephalic grafting in two patients with parkinsonism induced by 1-methyl-4-phenyl-1,2,3,6-tetrahydropyridine (MPTP). *N. Engl. J. Med.* **327**:1556–1563.
9. Smith, A.G. 2001. Embryo-derived stem cells of mice and men. *Annu. Rev. Cell Dev. Biol.* **17**:435–462.
10. Kawasaki, H., et al. 2000. Induction of midbrain dopaminergic neurons from ES cells by stromal cell-derived inducing activity. *Neuron.* **28**:31–40.
11. Kawasaki, H., et al. 2002. Generation of dopaminergic neurons and pigmented epithelia from primate ES cells by stromal cell-derived inducing activity. *Proc. Natl. Acad. Sci. U. S. A.* **99**:1580–1585.
12. Gage, F.H. 2000. Mammalian neural stem cells. *Science.* **287**:1433–1438.
13. Ohmachi, S., et al. 2000. FGF-20, a novel neurotrophic factor, preferentially expressed in the substantia nigra pars compacta of rat brain. *Biochem. Biophys. Res. Commun.* **277**:355–360.
14. Tonchev, A.B., Yamashima, T., Zhao, L., Okano, H.J., and Okano, H. 2003. Proliferation of neural and neuronal progenitors after global brain ischemia in young adult macaque monkeys. *Mol. Cell. Neurosci.* **23**:292–301.
15. Arenas, E. 2002. Stem cells in the treatment of Parkinson's disease. *Brain Res. Bull.* **57**:795–808.
16. Smidt, M.P., et al. 2000. A second independent pathway for development of mesencephalic dopaminergic neurons requires *Lmx1b*. *Nat. Neurosci.* **3**:337–341.
17. Ranjita, B., et al. 1997. Dopaminergic neurons intrinsic to the primate striatum. *J. Neurosci.* **17**:6761–6768.
18. Thomson, J.A., et al. 1995. Isolation of a primate embryonic stem cell line. *Proc. Natl. Acad. Sci. U. S. A.* **92**:7844–7848.
19. Suemori, H., et al. 2001. Establishment of embryonic stem cell lines from cynomolgus monkey blastocysts produced by IVF or ICSI. *Dev. Dyn.* **222**:273–279.
20. Lee, S.H., Lumelsky, N., Studer, L., Auerbach, J.M., and McKay, R.D. 2000. Efficient generation of midbrain and hindbrain neurons from mouse embryonic stem cells. *Nat. Biotechnol.* **18**:675–679.
21. Kim, J.H., et al. 2002. Dopamine neurons derived from embryonic stem cells function in an animal model of Parkinson's disease. *Nature.* **418**:50–56.
22. Morizane, A., Takahashi, J., Takagi, Y., Sasai, Y., and Hashimoto, N. 2002. Optimal conditions for in vivo induction of dopaminergic neurons from ES cells through stromal cell-derived inducing activity. *J. Neurosci. Res.* **69**:934–939.
23. Elsworth, J.D., et al. 1996. Early gestational mesencephalon grafts, but not later gestational mesencephalon, cerebellum or sham grafts, increase dopamine in caudate nucleus of MPTP-treated monkeys. *Neuroscience.* **72**:477–484.
24. Ohmachi, S., Mikami, T., Konishi, M., Miyake, A., and Ito, N. 2003. Preferential neurotrophic activity of fibroblast growth factor-20 for dopaminergic neurons through fibroblast growth factor receptor-1c. *J. Neurosci. Res.* **72**:436–443.
25. Ciccolini, F., and Svendsen, C.N. 1998. Fibroblast growth factor 2 (FGF-2) promotes acquisition of epidermal growth factor (EGF) responsiveness in mouse striatal precursor cells: identification of neural precursors responding to both EGF and FGF-2. *J. Neurosci.* **18**:7869–7880.
26. Kuhn, H.G., Winkler, J., Kempermann, G., Thal, L.J., and Gage, F.H. 1997. Epidermal growth factor and fibroblast growth factor-2 have different effects on neural progenitors in the adult rat brain. *J. Neurosci.* **17**:5820–5829.
27. Schuldiner, M., Tanuka, O., Itskovitz-Eldor, J., Melton, D.A., and Benvenisty, N. 2000. Effects of eight growth factors on the differentiation of cells derived from human embryonic stem cells. *Proc. Natl. Acad. Sci. U. S. A.* **97**:11307–11312.
28. Doudet, D.J., et al. 1998. 6-[18F]Fluoro-L-DOPA PET studies of the turnover of dopamine in MPTP-induced parkinsonism in monkeys. *Synapse.* **29**:225–232.
29. Elsworth, J.D., et al. 1994. Novel radioligands for the dopamine transporter demonstrate the presence of intrastriatal nigral grafts in the MPTP-treated monkey: correlation with improved behavioral function. *Exp. Neurol.* **126**:300–304.
30. Poyot, T., et al. 2001. Anatomic and biochemical correlates of the dopamine transporter ligand 11C-PE2I in normal and parkinsonian primates: comparison with 6-[18F]fluoro-L-dopa. *J. Cereb. Blood Flow Metab.* **21**:782–792.
31. Bankiewicz, K.S., et al. 1986. Hemiparkinsonism in monkeys after unilateral internal carotid artery infusion of 1-methyl-4-phenyl-1,2,3,6-tetrahydropyridine (MPTP). *Life Sci.* **39**:7–16.
32. Burns, R.S., et al. 1983. A primate model of parkinsonism: selective destruction of dopaminergic neurons in the pars compacta of the substantia nigra by N-methyl-4-phenyl-1,2,3,6-tetrahydropyridine. *Proc. Natl. Acad. Sci. U. S. A.* **80**:4546–4550.
33. Wenning, G.K., et al. 1997. Short- and long-term survival and function of unilateral intrastriatal dopaminergic grafts in Parkinson's disease. *Ann. Neurol.* **42**:95–107.
34. Betarbet, R., et al. 1997. Dopaminergic neurons intrinsic to the primate striatum. *J. Neurosci.* **17**:6761–6768.
35. Kordower, J.H., et al. 1996. Functional fetal nigral grafts in a patient with Parkinson's disease: chemoanatomic, ultrastructural, and metabolic studies. *J. Comp. Neurol.* **370**:203–230.
36. Martin, R.F., and Bowden, D.M. 2000. *Primate brain maps: structure of the macaque brain.* Volume 8. Elsevier. New York, New York, USA. 160 pp.
37. Schaltenbrand, G., and Wahren, W. 1977. *Atlas for stereotaxy of the human brain.* Georg Thieme Verlag. Stuttgart, Germany.
38. Björklund, A., et al. 2003. Neural transplantation for the treatment of Parkinson's disease. *Lancet Neurol.* **2**:437–445.
39. Jenner, P. 2003. The contribution of the MPTP-treated primate model to the development of new treatment strategies for Parkinson's disease. *Parkinsonism. Relat. Disord.* **9**:131–137.
40. Isacson, O., et al. 2001. Cell implantation therapies for Parkinson's disease using neural stem, transgenic or xenogeneic donor cells. *Parkinsonism. Relat. Disord.* **104**:205–212.
41. Collier, T.J., et al. 2002. Embryonic ventral mesencephalic grafts to the substantia nigra of MPTP-treated monkeys: feasibility relevant to multiple-target grafting as a therapy for Parkinson's disease. *J. Comp. Neurol.* **442**:320–330.
42. Björklund, A., and Lindvall, O. 2000. Cell replacement therapies for central nerovous system disorders. *Nat. Neurosci.* **3**:537–544.
43. Björklund, L.M., et al. 2002. Embryonic stem cells develop into functional dopaminergic neurons after transplantation in a Parkinson rat model. *Proc. Natl. Acad. Sci. U. S. A.* **99**:2344–2349.
44. Erdö, F., et al. 2003. Host-dependent tumorigenesis of embryonic stem cell transplantation in experimental stroke. *J. Cereb. Blood Flow Metab.* **23**:780–785.
45. Harkany, T., et al. 2004. Region-specific generation of functional neurons from naïve embryonic stem cells in adult brain. *J. Neurochem.* **88**:1229–1239.
46. Thomson, J.A., et al. 1998. Embryonic stem cell lines derived from human blastocysts. *Science.* **282**:1145–1147.
47. Reubinoff, B.E., et al. 2001. Neural progenitors from human embryonic stem cells. *Nat. Biotechnol.* **19**:1134–1140.
48. Zhang, S.C., Wernig, M., Duncan, I.D., Brustle, O., and Thomson, J.A. 2001. In vitro differentiation of transplantable neural precursors from human embryonic stem cells. *Nat. Biotechnol.* **19**:1129–1133.
49. Nagano, Y., et al. 2003. Siah-1 facilitates ubiquitination and degradation of Synphilin-1. *J. Biol. Chem.* **278**:51504–51514.
50. Sabo, J., and Cowan, W.M. 1984. A stereotaxic atlas of the brain of the cynomolgus monkey (Macaca fascicularis). *J. Comp. Neurol.* **222**:265–300.
51. Akai, T., Ozawa, M., Yamaguchi, M., Mizuta, E., and Kuno, S. 1995. Combination treatment of the partial D2 agonist terguride with the D1 agonist SKF 82958 in 1-methyl-4-phenyl-1,2,3,6-tetrahydropyridine-lesioned parkinsonian cynomolgus monkeys. *J. Pharmacol. Exp. Ther.* **273**:309–314.
52. Patlak, C.S., and Blasberg, R.G. 1985. Graphical evaluation of blood-to-brain transfer constants from multiple-time uptake data. *J. Cereb. Blood Flow Metab.* **5**:584–590.

Journal of Cerebral Blood Flow & Metabolism (2005), 1–16

www.jcbfm.com

Rapid quantitative measurement of $CMRO_2$ and CBF by dual administration of ^{15}O-labeled oxygen and water during a single PET scan—a validation study and error analysis in anesthetized monkeys

Nobuyuki Kudomi, Takuya Hayashi, Noboru Teramoto, Hiroshi Watabe, Naoki Kawachi, Youichirou Ohta, Kyeong Min Kim and Hidehiro Iida

Department of Investigative Radiology, Advanced Medical-Engineering Center, National Cardiovascular Center-Research Institute, Fujishirodai, Suita, Osaka, Japan

Cerebral blood flow (CBF) and rate of oxygen metabolism ($CMRO_2$) may be quantified using positron emission tomography (PET) with ^{15}O-tracers, but the conventional three-step technique requires a relatively long study period, attributed to the need for separate acquisition for each of $^{15}O_2$, $H_2^{15}O$, and $C^{15}O$ tracers, which makes the multiple measurements at different physiologic conditions difficult. In this study, we present a novel, faster technique that provides a pixel-by-pixel calculation of CBF and $CMRO_2$ from a single PET acquisition with a sequential administration of $^{15}O_2$ and $H_2^{15}O$. Experiments were performed on six anesthetized monkeys to validate this technique. The global CBF, oxygen extraction fraction (OEF), and $CMRO_2$ obtained by the present technique at rest were not significantly different from those obtained with three-step method. The global OEF (gOEF) also agreed with that determined by simultaneous arterio-sinus blood sampling ($gOEF_{A-V}$) for a physiologically wide range when changing the arterial $PaCO_2$ ($gOEF = 1.03 gOEF_{A-V} + 0.01$, $P < 0.001$). The regional values, as well as the image quality were identical between the present technique and three-step method for CBF, OEF, and $CMRO_2$. In addition, a simulation study showed that error sensitivity of the present technique to delay or dispersion of the input function, and the error in the partition coefficient was equivalent to that observed for three-step method. Error sensitivity to cerebral blood volume (CBV) was also identical to that in the three-step and reasonably small, suggesting that a single CBV assessment is sufficient for repeated measures of $CBF/CMRO_2$. These results show that this fast technique has an ability for accurate assessment of $CBF/CMRO_2$ and also allows multiple assessment at different physiologic conditions.
Journal of Cerebral Blood Flow & Metabolism advance online publication, 4 May 2005; doi:10.1038/sj.jcbfm.9600118

Keywords: CBF; $CMRO_2$; dual tracer; PET; rapid measurement

Introduction

Positron emission tomography (PET) allows the quantitative measurement of regional cerebral blood flow (CBF) and the rate of oxygen metabolism ($CMRO_2$), which has enabled us to understand the pathophysiologic basis of cerebrovascular disorders. These measurements are achieved using a protocol involving separate PET scans, one after the administration of each of three distinct ^{15}O-labeled radioactive tracers: $H_2^{15}O$ or $C^{15}O_2$ for CBF, $^{15}O_2$ for $CMRO_2$, and $C^{15}O$ for cerebral blood volume (CBV) (Frackowiak *et al*, 1980*a*, *b*; Mintun *et al*, 1984; Lammertsma and Jones, 1983). However, the complex nature of this procedure and its relatively long protocol often limit its applicability and also makes it difficult to perform at different physiologic conditions.

Quantitative images of CBF and $CMRO_2$ created with PET are calculated based on a single-tissue compartment model of oxygen and water kinetics

Correspondence: Dr N Kudomi, Department of Investigative Radiology, Advanced Medical-Engineering Center, National Cardiovascular Center-Research Institute, 5-7-1, Fujishirodai, Suita, Osaka 565-8565, Japan.
E-mail: kudomi@ri.ncvc.go.jp
The present work was supported by the Program for Promotion of Fundamental Studies in Health Science of the Organization for Pharmaceuticals and Medical Devices Agency of Japan (PMDA), by Kobe Cluster, Ministry of Education, Culture, Sports, Science, and Technology (MEXT), and by the Japan Cardiovascular Research Foundation.
Received 13 May 2004; revised 19 December 2004; accepted 12 January 2005

(Frackowiak *et al*, 1980*a*, *b*; Mintun *et al*, 1984; Lammertsma and Jones, 1983). The steady-state method (Subramanyam *et al*, 1978; Lammertsma *et al*, 1982; Correia *et al*, 1985; Okazawa *et al*, 2001*a*, *b*) has been used in a number of studies in which quantitative images are estimated from data acquired while in the steady state reached during continuous inhalation of $C^{15}O_2$ and $^{15}O_2$. This method can be used using a simple procedure and mathematical formula, but still has several limitations. A prolonged data-acquisition period (approximately 1 h) is required, and the procedure is sensitive to error sources such as statistical noise and tissue heterogeneity (Lammertsma *et al*, 1982; Correia *et al*, 1985). An additional drawback is the relatively high level of radiation exposure required to reach the steady state.

An alternative autoradiographic method (ARG) using only short administration times for each of the three tracers (three-step ARG) has been developed (Mintun *et al*, 1984) and subsequently simplified and optimized (Iida *et al*, 1993; Sadato *et al*, 1993; Hatazawa *et al*, 1995; Shidahara *et al*, 2002; Hattori *et al*, 2004). Cerebral blood flow images can be obtained by an $H_2^{15}O$ autoradiographic method, using a PET counts-versus-CBF nomogram, which follows a simple look-up table procedure (Raichle *et al*, 1983; Herscovitch *et al*, 1983; Kanno *et al*, 1987); the quantitative accuracy of these images is improved when input delay and dispersion are corrected (Iida *et al*, 1986, 1988). Rate of oxygen metabolism and the oxygen extraction fraction (OEF) can be estimated using data acquired during $^{15}O_2$ inhalation, but must be corrected for clearance of radioactivity associated with CBF (Mintun *et al*, 1984), CBV, and the level of recirculating radioactive water (Iida *et al*, 1993). Although the total time required for three-step ARG is less than that of the steady-state method, it still requires at least half an hour, with a large part of this period spent waiting for radioactive decay between PET scans (more than 10 mins).

There have been other attempts to obtain CBF and $CMRO_2$ images more rapidly (Huang *et al*, 1986; Holden *et al*, 1988; Meyer *et al*, 1987; Ohta *et al*, 1992; Ho and Feng, 1999). Mathematical refinement has allowed images to be generated from data from a single scan alone on a bolus inhalation of $^{15}O_2$. The quality of the image suffers, however, from statistical noise because of the lack of predictability of the multiple parameters of CBF, $CMRO_2$, and the arterial vascular compartment (V_0) and the limited acquisition time (Meyer *et al*, 1987; Ohta *et al*, 1992). Therefore, this technique has not been generally applied in clinical settings, but has been used primarily for research purposes (Fujita *et al*, 1999; Vafaee and Gjedde, 2000; Okazawa *et al*, 2001*a*, *b*; Mintun *et al*, 2002).

In this study, we have developed a novel, rapid PET technique called the dual-tracer ARG method (DARG) that involves a single session of PET scan during which two tracers of $^{15}O_2$ and $H_2^{15}O$ are sequentially administered. This approach can shorten the total study period for the CBF and $CMRO_2$ measurement as compared with the three-step ARG, while maintaining the image quality and quantitative accuracy. A new formulation was derived so that the residual radioactivity of the first tracer is accounted for in the subsequent portion of the dynamic PET scan. We have then tested feasibility of this technique in an experiment on six anesthetized monkeys. A set of simulation was also performed to evaluate error sensitivity to possible error sources.

Materials and methods

Theory

The DARG protocol consists of a single dynamic PET scan conducted during the sequential administration of $H_2^{15}O$ and $^{15}O_2$ in a short time interval. To calculate values of CBF, OEF, and $CMRO_2$ from these data, a new mathematical formula was derived based on a previously described single-tissue compartment model (Mintun *et al*, 1984). The formula was redesigned to be applicable to data obtained after the administration of tracers in either order ($H_2^{15}O$ injection followed by $^{15}O_2$ inhalation ($H_2^{15}O$–$^{15}O_2$) or $^{15}O_2$ inhalation followed by $H_2^{15}O$ injection ($^{15}O_2$–$H_2^{15}O$)). Schematic time courses of blood and tissue radioactivity during DARG are shown in Figure 1. Based on the single-tissue compartment model, the total radioactivity in the

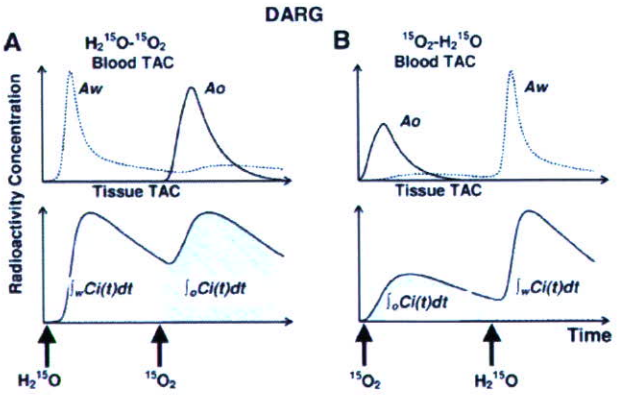

Figure 1 Schematic TACs of arterial blood and tissue for the sequential administration of dual tracers in DARG: (**A**) $H_2^{15}O$ followed by $^{15}O_2$ inhalation ($H_2^{15}O$–$^{15}O_2$), and (**B**) $^{15}O_2$ followed by $H_2^{15}O$ ($^{15}O_2$–$H_2^{15}O$). (Upper) solid line, arterial blood TAC of $^{15}O_2$ (A_o); broken line, arterial blood TAC of $H_2^{15}O$ including both administered and recirculating (A_w); (lower) solid line, whole brain tissue TAC. The area under the curve (shaded) corresponds to the PET data integrated after the administration of $^{15}O_2$ ($\int_o Ci(t)\,dt$) and after $H_2^{15}O$ ($\int_w Ci(t)\,dt$) that was used for the calculation of functional values. TAC, time activity curve; DARG, dual tracer autoradiographic method.

tissue, $Ci(t)$ in Bq/mL, after $^{15}O_2$ or $H_2^{15}O$ administration can be expressed as

$$Ci(t) = fA_w(t) \otimes e^{-(f/p)t} + EfA_o(t) \otimes e^{-(f/p)t} + V_B R_{Hct} \times (1 - EFv)A_o(t) + V_A A_w(t) \quad (1)$$

where $A_o(t)$ and $A_w(t)$ denote the arterial input function for oxygen and water in Bq/mL, f is CBF in mL 100/g min, E is the OEF, p is the blood/brain partition coefficient for water in mL/g, V_B or V_A is the total or arterial part of cerebral blood volume, respectively, R_{Hct} is the small-to-large vessel hematocrit ratio, Fv is the effective venous fraction, and $\otimes$ indicates the convolution integral. Note that equation (1) describes the kinetics of radioactivity and is valid after the administration of either ^{15}O or $H_2^{15}O$ or after the administration of both. The first term on the right-hand side describes the amount of water entering the tissue, including both administrated and recirculating water. The second represents the amount of oxygen that enters the tissue and is immediately metabolized to water. The third and the fourth terms express the radioactivity of $^{15}O_2$ and $H_2^{15}O$ in blood vessels, respectively. In the present study, we assumed that the last term is negligibly small compared with the radioactivity in tissue according to the previous study (Iida *et al*, 2000). Then, we have

$$Ci(t) = fA_w(t) \otimes e^{-(f/p)t} + EfA_o(t) \otimes e^{-(f/p)t} + V_B R_{Hct}(1 - EFv)A_o(t) \quad (2)$$

To produce pixel-by-pixel functional maps using a look-up table procedure, the formula was rearranged as follows. Equation (2) was integrated for the periods of $H_2^{15}O$ ($\int_w dt$) and $^{15}O_2$ administration ($\int_O dt$):

$$\int_W Ci(t)\,dt = f\int_W A_w \otimes e^{-(f/p)t}\,dt + Ef\int_W A_o \otimes e^{-(f/p)t}\,dt + V_B R_{Hct}(1 - EFv)\int_W A_o(t)\,dt \quad (3)$$

$$E = \frac{\int_O Ci(t) - f\int_O A_w \otimes e^{-(f/p)t}\,dt - V_B R_{Hct}\int_O A_O\,dt}{f\int_O A_w \otimes e^{-(f/p)t}\,dt - V_B R_{Hct} Fv \int_O A_O\,dt} \quad (4)$$

In these equations, $\int_w Ci(t)dt$ and $\int_o Ci(t)dt$ correspond to acquired PET data summed after $H_2^{15}O$ and $^{15}O_2$ administration, respectively (Figure 1). Note that the radioactivity of the first tracer remaining during data acquisition for the second tracer is already modeled in each equation. In the case of $^{15}O_2$–$H_2^{15}O$, the amount of residual radioactivity from $^{15}O_2$ in data obtained during the H_2O segment (equation (3)) is expressed in the second and third terms on the right-hand side. Likewise, for $H_2^{15}O$–$^{15}O_2$, the residual amount of $H_2^{15}O$ found in the data for the O_2 segment (equation (4)) is represented by the first term on the right-hand side. Equation (4) can be rewritten as follows:

$$E = \frac{\int_O Ci(t) - f\int_O A_w \otimes e^{-(f/p)t}\,dt - V_B R_{Hct}\int_O A_O\,dt}{f\int_O A_O \otimes e^{-f/pt}\,dt - V_B R_{Hct} Fv \int_O A_O\,dt} \quad (5)$$

Substituting equation (5) into equation (3), we obtain

$$\int_W Ci(t)\,dt = f\int_W A_w \otimes e^{-(f/p)t}\,dt + V_B R_{Hct}\int_W A_o(t)\,dt + (f\int_W A_o \otimes e^{-(f/p)t}dt - V_B R_{Hct} Fv \int_W A_o(t)\,dt = \frac{\int_O Ci(t) - f\int_O A_w \otimes e^{-(f/p)t}\,dt - V_B R_{Hct}\int_O A_O\,dt}{f\int_O A_O \otimes e^{-(f/p)t}\,dt - V_B R_{Hct} Fv \int_O A_O\,dt} \quad (6)$$

Using equation (6), f can be estimated using a look-up table procedure based on the observed PET data ($\int_w Ci(t)dt$ and $\int_o Ci(t)dt$, V_B) and the blood input functions (A_o and A_w), as long as fixed values are assumed for P, Fv, and R_{Hct}. Next, E can be calculated using equation(5). Rate of oxygen metabolism is then calculated from the estimated f and E, and the measured arterial oxygen content.

Positron Emission Tomography Experiments in an Animal System

We measured CBF and $CMRO_2$ using PET in six normal monkeys (*Macaca fascicularis*; body weight = 5 kg) under stable anesthesia. The PET protocol for this study was designed to validate the global values of CBF (gCBF), $CMRO_2$ (g$CMRO_2$), and OEF (gOEF) generated using DARG by comparing them to those obtained using three-step ARG and the gOEF value measured by simultaneous arterial and cerebral sinus (A–V) blood sampling ($gOEF_{A\text{-}V}$). In all six animals, we performed three-step ARG, two sets of DARG ($H_2^{15}O$–$^{15}O_2$ and $^{15}O_2$–$H_2^{15}O$), and A–V sampling during normocapnia (Figure 2). In three of the six animals, A–V sampling and DARG with $^{15}O_2$–$H_2^{15}O$ were performed simultaneously not only during normocapnia ($PaCO_2 \cong 40$ mm Hg) but also while $PaCO_2$ was graded (by changing the respiratory rate) at different three levels: hypocapnia ($PaCO_2 < 33$ mm Hg), mild hypercapnia ($45 < PaCO_2 < 50$ mm Hg), and deep hypercapnia ($PaCO_2 > 50$ mm Hg). Animals were maintained and handled in accordance with the guidelines for animal research outlined in Human Care and Use of Laboratory Animals (Rockville, National Institute of Health/Office for Protection from Research Risks, 1996). The study protocol was approved by Subcomittee for Laboratory Animal Welfare, National Cardiovascular Center.

Anaesthesia was induced with ketamine (10 mg/kg, intramuscularly) and maintained by intravenous propofol

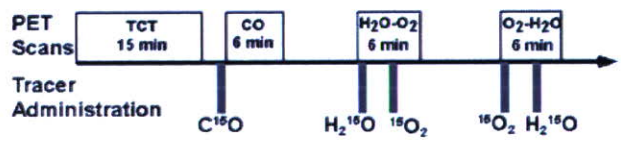

Figure 2 Animal study protocol. After a 15-min transmission scan (TCT), a 6-min emission scan was performed after a 30-sec inhalation of $C^{15}O$. Next, two 6-min dynamic scans with the sequential administration of $H_2^{15}O$ and $^{15}O_2$, with 3-min interval, were performed. The order of two tracers was alternated between the first ($H_2^{15}O$–$^{15}O_2$) and the second ($^{15}O_2$–$H_2^{15}O$) scans across subjects.

(4 mg/kg h) and vecuronium (0.05/mg kg h) during the experiment. Animals were intubated and their respiration was controlled by an anaesthetic ventilator (Cato; Drager, Germany) providing a gas mixture of 24% O_2 and 76% N_2. A catheter was inserted into the femoral artery for blood sampling and into the anterior tibial vein for injection of $H_2^{15}O$ and anaesthetic agents. Arterial blood pressure, heart rate, and endotidal CO_2 levels were continuously monitored throughout the procedure. Arterial blood gas analysis was performed to measure the O_2 content and the $PaCO_2$ level. To assist in data analysis, all animals underwent 3D T1-weighted magnetic resonance imaging (MRI) (IR-FSPGR, $TR = 9.4$ ms, $TE = 2.1$ ms, $TI = 600$ ms) using a 3 T MRI scanner (Signa LX VAH/I, GE, Milwaukee, USA) in advance of the PET study.

Positron emission tomography acquisition was performed in 2D mode using a PET scanner (ECAT HR, Siemens-CTI, Knoxville, USA). After a 900-sec transmission scan with a rotating ^{68}Ge–^{68}Ga rod source, the dynamic scan began after the inhalation of $C^{15}O$. After 10 mins of radioactivity decay, $^{15}O_2$ (2200 MBq) and then $H_2^{15}O$ (370 MBq) were administered in sequence, each for a 3-min interval during a 6-min dynamic PET scan ($H_2^{15}O$–$^{15}O_2$) consisting of 63 frames of gradually increasing individual durations (24×5, 6×10, 30×5, and 3×10 secs). We intended to increase the number of 5-sec frames during the second tracer-appearance period, because of possible delay of the tracer administration attributed to the synthesizer and/or injector. After 10 mins, a scan for $^{15}O_2$–$H_2^{15}O$ was performed using the same dynamic data acquisition protocol. The order of $^{15}O_2$–$H_2^{15}O$ or $H_2^{15}O$–$^{15}O_2$ was randomized across subjects. The $^{15}O_2$ was inhaled for 20 secs in a slow bolus supplied via a polyethylene tube connected to the ventilator, and the $H_2^{15}O$ was injected over a period of 30 secs via the anterior tibial vein, accompanied by an additional bolus of saline for flushing. For the three animals that received variations in $PaCO_2$, at least 30 mins were allotted to reach a steady-state $PaCO_2$, after which $^{15}O_2$–$H_2^{15}O$ DARG was performed.

To obtain an arterial time–activity curve, arterial blood was withdrawn continuously from the femoral artery through a catheter (0.6-mm inner diameter) using a syringe pump (Harvard Apparatus, model 55–2309) with a withdraw speed of 0.45 mL/min, and the whole-blood radioactivity concentration was measured using a GSO input function monitor system (Kudomi *et al*, 2003). We also measured the radioactivity concentration in plasma to estimate the ^{15}O-labeled water concentration produced as a metabolite of $^{15}O_2$, for which 0.2 mL of blood was centrifuged after manual sampling at eight time points: 30, 50, 70, 90, 110, 130, 160, and 190 secs after $^{15}O_2$ inhalation. The radioactivity for plasma and whole blood was measured by a well counter (NaI(Tl) scintillation counter, Aloka, Japan) cross-calibrated to the PET scan, and expressed as Bq/mL.

Arterial–Sinus Blood Sampling

We performed arterial–sinus blood sampling to obtain a global OEF ($gOEF_{A-V}$) based on the Kety–Schmidt method (Kety and Schmidt, 1948). The sinus blood was sampled through a 3F catheter, which was introduced via the femoral vein to the cerebral sinus using a high-resolution digital X-ray imaging system (GE Medical System, USA). To avoid mixing with venous blood draining from extracranial tissues, the tip of the catheter was carefully placed at the angle of the cerebral sigmoid and transverse sinuses, and its position was confirmed at the conclusion of each PET protocol. We sampled 0.2 mL of arterial and sinus blood simultaneously during each DARG PET scan and measured their oxygen content (C_aO_2 and C_vO_2, respectively). The $gOEF_{A-V}$ was calculated as follows:

$$gOEF_{A-V} = (C_aO_2 - C_vO_2)/C_aO_2$$

Data Processing

Corrections for dead time, the radioactive decay, and normalization of detectors were performed using the sinogram-based method described previously (Shidahara *et al*, 2002). Part of the corrected sinogram for the $H_2^{15}O$–$^{15}O_2$ or $^{15}O_2$–$H_2^{15}O$ scan was summed for each period of labeled water (120 secs from the start time of water injection, or effectively 90 secs after the rise time of the tissue TAC), and oxygen intake (180 secs from the start time of oxygen inhalation). The summed images were corrected for attenuation using transmission data, and were reconstructed using the filtered-back-projection method with a 4-mm Gaussian filter. A reconstructed image consisted of a $128 \times 128 \times 47$ matrix with a pixel size of $1.1 \times 1.1 \times 3.38$ mm. In addition, dynamic sinograms for the $H_2^{15}O$–$^{15}O_2$ and $^{15}O_2$–$H_2^{15}O$ scans were reconstructed with same conditions as above and used for a nonlinear least-squares fitting (NLF) analysis.

To correct for the delay between the brain and blood TACs, the whole brain TAC was obtained from the corrected dynamic sinograms (Shidahara *et al*, 2002). The delay was estimated based on a method previously described (Iida *et al*, 1988). Briefly, three parameters, K_1, k_2, and delay (Δt), were determined using whole brain and blood TACs around the period of $H_2^{15}O$ injection with an NLF procedure (Iida *et al*, 1988; Shidahara *et al*, 2002). The dispersion time constant was fixed at 3 secs (Shidahara *et al*, 2002).

To compute CBF, OEF, and $CMRO_2$ as described above, it is necessary to obtain separated $^{15}O_2$ and $H_2^{15}O$ input functions (A_o and A_w) from the measured arterial TAC, because the arterial blood TAC measured during the second phase of the scan reflects not only the radioactivity of the second tracer but also the residual activity of the first. For the $H_2^{15}O$–$^{15}O_2$ protocol, we first estimated the TAC for the residual radioactivity from the first tracer ($H_2^{15}O$) administration remaining during the second period by extrapolating the arterial TAC of the first phase by a model of input function (Kudomi *et al*, 2002). We then subtracted it from the measured total arterial TAC in the second phase to obtain a TAC for the second tracer. Second, the metabolic product (recirculating water) following $^{15}O_2$ administration was estimated using the plasma radioactivity measured during the phase of $^{15}O_2$